Arab J Sci Eng (2015) 40:3417–3427
DOI 10.1007/s13369-015-1776-9

RESEARCH ARTICLE - CIVIL ENGINEERING

Experimental and Numerical Investigation on Thin-Walled Single and Starred Angle Sections Under Compression

G. Beulah Gnana Ananthi[1] · **S. Vishuvardhan**[2] · **G. M. Samuel Knight**[1]

Received: 9 October 2014 / Accepted: 13 July 2015 / Published online: 26 July 2015

Abstract This paper presents experimental and numerical investigations on the behaviour of thin-walled cold-formed steel single and starred angles with lips as stub and short columns, subjected to axial compression. A nonlinear finite element model was developed and verified against the ball- and bolted-end conditions. The specimens are modelled precisely for the numerical investigation using finite element analysis as done in the column tests carefully under-controlled. Both geometric and material nonlinearities are included in the finite element model. The predicted column strengths by the numerical analysis are compared with the design column strengths calculated using the North American Standards for cold-formed steel structures. It is shown that the design column strengths calculated from the specification are generally conservative for cold-formed steel angle sections. Results from the FEA correlate well with experimental data, NAS-2007 and BS: 5950 (Part 5) predictions.

Keywords Cold-formed steel · Stub columns · Single and starred angles · Finite element analysis · Codal provisions

✉ G. Beulah Gnana Ananthi
beulahsap@gmail.com

[1] Division of Structural Engineering, CEG Campus, Anna University, Chennai 600025, India

[2] CSIR - Structural Engineering Research Centre, CSIR Campus, Taramani, Chennai, India

Abbreviations

FEA	Finite element analysis
P_{EXP}	Experimental ultimate load
P_{FEA}	FEA ultimate load
P_{BS}	Ultimate load predicted by the British Standards
P_{NAS}	Ultimate load predicted by the North American Standards
λ	Slenderness ratio

1 Introduction

Cold forming is a process where steel members are manufactured by rolling or shaping the steel after it is cold. Thin sheet steel products are extensively used in building industry and range from purlins to roof materials and floor decking. Generally, these are available for use as basic building elements for assembly at site or as pre-fabricated frames or panels. These thin steel sections are cold-formed, i.e. their manufacturing process involves forming steel sections in a cold state (i.e. without application of heat) from steel sheets of uniform thickness. The thickness of steel sheet used in cold-formed construction is usually 1–3 mm. Much thicker material up to 8 mm can be formed if pre-galvanised material is not required for the particular application. Sustained research and continuous upgradation of design codes contribute to the maximum utilisation of these sections for construction.

Angles are the most common structural shape found in almost any structure due to their simplicity and ease of fabrication and erection. Single angles are usually used as web members in steel joist and trusses, members of latticed transmission towers or communication structures and bracing members to provide lateral support to the main members. Angles welded in the form of starred section, which is dou-

bly symmetric, are used widely as the legs of transmission line towers. It is customary to assume the connections either as frictionless pins or as fully rigid connections.

There are many codal specifications for the design of cold-formed steel such as BS: 5950 [1] and NAS Manual [2] issued by various countries. Many times, evaluating the ultimate load-carrying capacity is a tedious process since all these codes involve empirical formulas. Codal provisions also lack in clarity with uncommon sections. The basis for the determination of member capacities of cold-formed steel sections is either allowable stress design (ASD) or the limit state design referred to as load and resistance factor design (LRFD). Most of the specifications, namely British Standards (BS) and the North American Standards have switched over from ASD to LRFD. The aim of this study is to investigate experimentally, theoretically and numerically the elastic and inelastic behaviour of thin-walled angle columns subjected to the axial loading. Young and Chen [3] presented a test programme on cold-formed steel non-symmetric lipped angle columns. The test strengths are compared with the design strengths calculated using the North American Standards for the design of cold-formed steel structural members. It was shown that the design strengths are generally quite conservative. An experimental investigation of cold-formed steel lipped angle concentrically loaded compression members was studied by Young [4]. The test strengths were compared with the design strengths predicted using the North American Standards and Australian/New Zealand Standard for cold-formed steel structures. It was concluded that the design strengths predicted by the specification and standard were conservative without considering the required additional bending moment using an eccentricity of 1/1000 of the column length. Young and Ellobody [5] have investigated the behaviour and design of cold-formed steel unequal angle columns. The column strengths obtained from the parametric study were compared with the design strengths calculated using the North American Standards for cold-formed steel structural members. It was shown that the current design rules are generally unconservative for short and intermediate column lengths for the unequal angles. Therefore, design rules of cold-formed steel unequal angle columns are proposed.

Young and Ellobady [6] described the finite element analysis of cold-formed steel equal lipped angle compression members. The column strengths predicted by the finite element model were compared with the design strengths calculated using the North American Standards and Australian/New Zealand Standard for cold-formed steel structures, as well as compared with the design strengths obtained from proposed design rules. It was shown that the proposed design strengths accurately predicted the column strengths for non-slender lipped angle columns. Yi and Chantel [7] studied a total of 26 steel unequal-leg angle specimens tested under eccentric compression and have suggested that for angles subjected to major principal axis bending causing the angle short leg in compression, the presence of moment, in some cases, resulted in the angle ultimate load higher than its concentric compressive capacity. Silvestre et al. [8] presented procedures for the design of fixed- and pin-ended equal-leg angle columns with short-to-intermediate lengths. The set of experimental results is comprised of 41 fixed-ended columns and 37 pin-ended columns, and the numerical results obtained include 89 fixed-ended columns and 28 pin-ended columns; various cross section dimensions, lengths and yield stresses are considered. It was shown that the proposed DSM approach leads to accurate ultimate strength estimates for short-to-intermediate columns covering a wide slenderness range.

Rasmussen [9] addresses the design of angle section columns whose legs were slender and thus subject to local buckling in their ultimate limit state. He described a design method for slender equal-leg angles which ignore torsion in determining the overall buckling stress and use recently presented effective width equations to accurately determine the bending capacity of angle sections, as required in the beam column design approach. Shifferawa and Schafer [10] explored the significant post-buckling reserve in global buckling that has been observed in tests on cold-formed steel angle columns and provided sign guidance for locally slender cold-formed steel lipped and plain angle columns with fixed-end boundary conditions. New design procedures are recommended for strength prediction of cold-formed steel angle columns with fixed-end boundary conditions.

2 Experimental Investigations

2.1 Material Properties

The specimens used in the present investigation are fabricated from cold-formed steel sheets of various thicknesses 2.00 and 3.15 mm with various material properties. The yield strength, ultimate tensile strength and percentage elongation of the material are determined by tensile coupon tests conforming to ASTM A 370. The yield stress was determined by the offset method since cold-formed steel is gradually yielding. The yield point of the steels recommended for cold forming by the NAS ranges from 172 to 482 N/mm^2. Similarly, the ultimate tensile strength of the steel specified in the NAS ranges from 289 to 584 N/mm and the ratio of tensile strength to yield strength ranges from 1.21 to 1.8. The minimum percentage elongation recommended by the NAS ranges from 12 to 27. The average values of Young's modulus, yield stress, ultimate stress and percentage elongation of the steel used in the present study for different specimens are shown in Table 1.

Table 1 Material properties of the steel

Sl. no.	Specimen ID LA-b-b-d-t (mm)	λ	Modulus of elasticity E (MPa)	f_y	Ultimate stress f_u (MPa)	% Elongation	End condition
1	LA-35-35-15-2	15, 20, 25	179	205	300	13	Ball
2	LA-40-40-15-2	15, 30	211	415	495	10	Ball
3	LA-40-40-15-3.15	20, 30	201	250	350	11	Ball
4	LA-60-60-15-2	20, 30	210	310	410	10	Bolted
5	LA-60-60-25-2	20, 30	210	310	365	26	Bolted
6	LA-60-60-15-3.15	20, 30	208	250	365	26	Bolted
7	LA-60-60-25-3.15	20, 30	208	250	365	26	Bolted
8	LA-70-70-15-3.15	20, 30	208	250	365	26	Bolted
9	LA-70-70-25-3.15	20, 30	208	250	365	26	Bolted

Fig. 1 Details of specimens

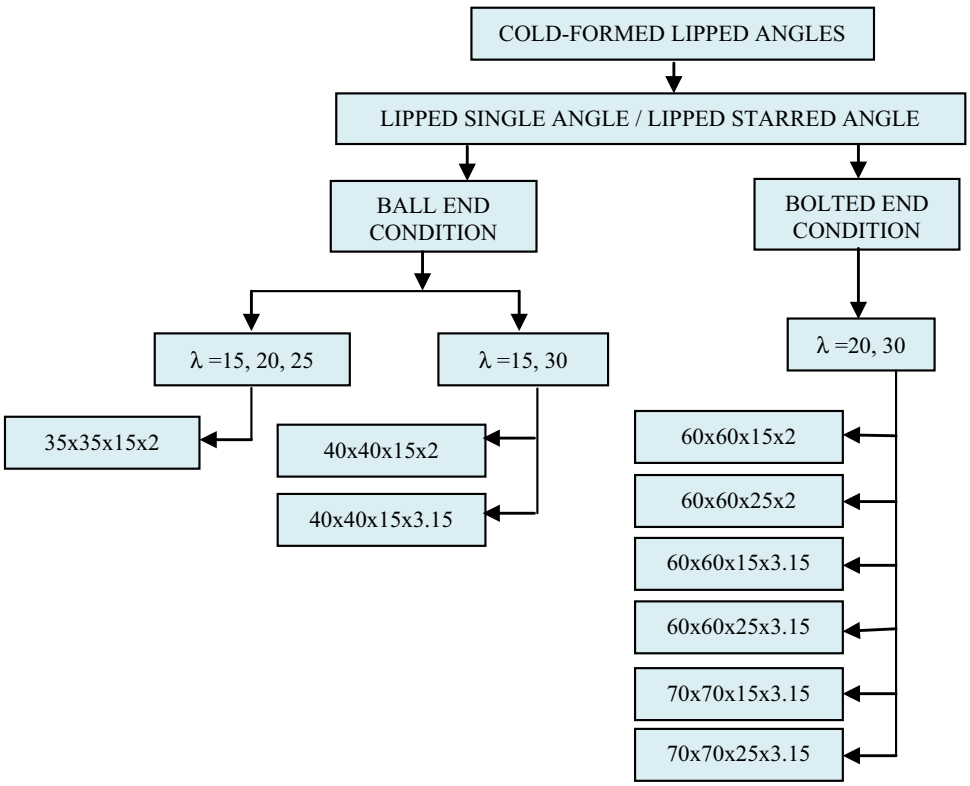

2.2 Test Specimen

Each specimen was manufactured by press braking method to the required shape from the steel sheets, and then they are processed. Single angles of required sizes are obtained first, and then the starred angles are prepared by welding the two single angles of same size as per NAS Manual-2007 [2]. To facilitate the axial loading process, the end plates are milled flat and welded on both ends of the stub and short columns. Thirty-eight experiments are done on single and starred angles with two different boundary conditions. The different cross sections of the specimens considered for the study are shown in Fig. 1. All the specimens are tested either as stub columns or as short columns. Twenty specimens are tested as stub columns of slenderness ratio 10, 15 and 20. Stub columns are specimens whose height is not less than three times the largest dimension of the section and not more than twenty times the least radius of gyration as per BS 5950-Part-5 [1]. Eighteen tests were done on short columns of slenderness ratio 25 and 30.

The specimens are labelled such that the type of angles, legs of the angles, lip depth and the thickness can be understood from the label as shown in Fig. 2.

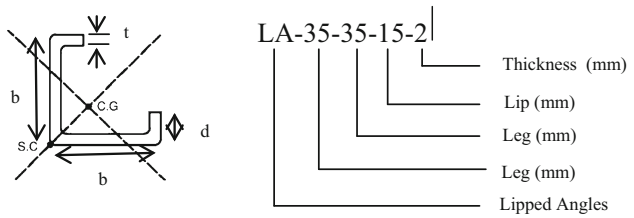

Fig. 2 Specimen labelling

2.3 Ball-End Condition

The ball-end conditions are fabricated by welding the sections to an end bearing plate of 6 mm thick and in turn connected to a pair of flat bearing plates of size varying from 60 × 60 mm to 120 × 120 mm. The assembly consisted of two end plates of 16 mm thick with a spherical groove in between to accommodate a ball of 40 mm diameter at both ends as shown in Figs. 3 and 4.

2.4 Bolted-End Condition

For the bolted condition, the specimens are bolted to two hot-rolled angles of size varying from 50 × 50 × 6 mm to 75 × 75 × 6 mm connected to 20-mm-thick base plate of size 200 × 200 mm as shown in Figs. 3 and 5. Bolt holes of 12 mm nominal diameter are made in the specimens to connect to the gusset angles as specified by NAS manual-2007 [2].

2.5 Test Set-Up

The compression tests are carried out using a column testing machine. The specimens are mounted between the platens, and its verticality was checked. The specimens are tested under axial compression with two different end conditions, viz. ball-end condition and bolted-end condition. For each test, the axial load was increased at a relatively faster rate in the elastic range and at a slower rate in the plastic range till the specimen collapsed. Dial gauges are placed at the mid-height and also at the one-fourth of the height of section with their tips touching the web and flange of the specimens to measure the lateral deflections. One dial gauge was placed with its tip touching the movable head of the column testing machine to measure the axial shortening of the test specimens. Figure 5 shows the experimental set-up.

3 Finite Element Model

An experimental investigation can be supplemented with a numerical method of predicting the behaviour within the acceptable accuracy limit. There are many practical engineering problems for which one cannot obtain exact solutions. The finite element method (FEM) is a numerical technique to obtain approximate solutions to a wide variety of engineering problems where the variables are related by means of algebraic, differential and integral equations. As the cold-formed

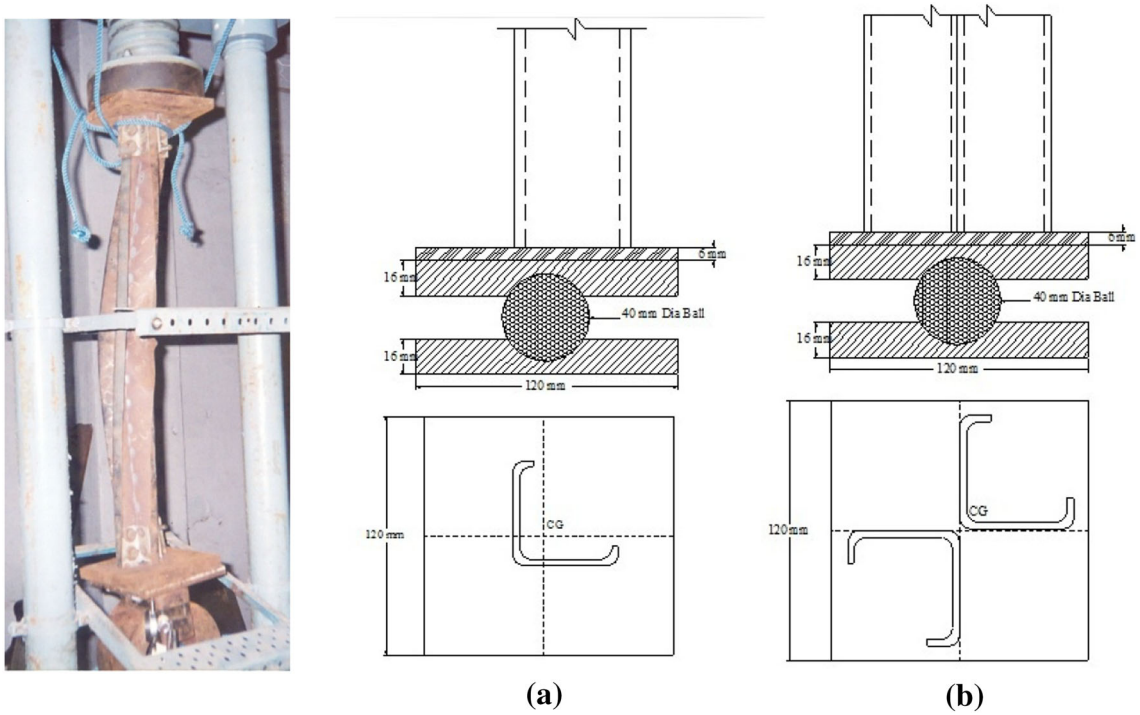

Fig. 3 Details of ball-end condition. **a** Single angle, **b** starred angle

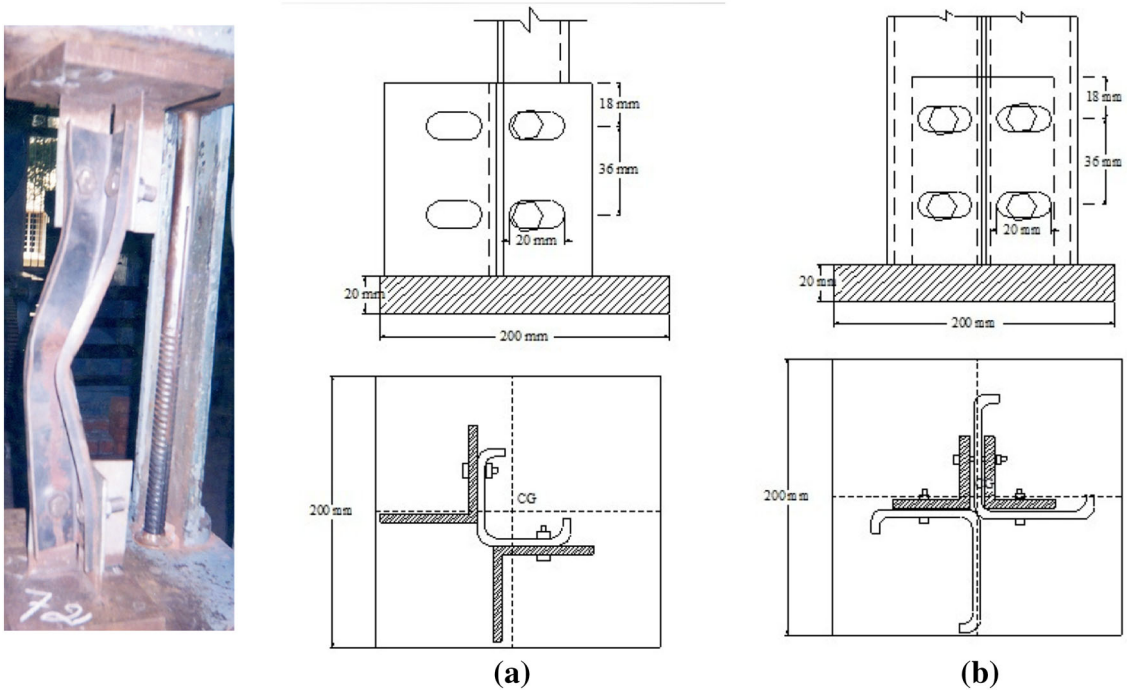

Fig. 4 Details of bolted-end condition. **a** Single angle, **b** starred angle

Fig. 5 Experimental set-up. **a** Single angle, **b** starred angle

steel sections are very thin as compared with their other dimensions, plate–shell element (S4R) available in ABAQUS software was found to yield results with acceptable accuracy for modelling. The analytical studies include static, stability and nonlinear analysis. The model validation was done with S4R element which is a 4-noded doubly curved shell element with reduced integration and hourglass control using five degrees of freedom per node. C3D8R, a solid element which is defined by an 8-noded linear brick, with reduced integration and hourglass control, was used to model the end plates which were used to transfer the load to the channel column section. A high mesh density usually increases the accuracy of the results obtained at the expense of computation time, while low mesh density can lead to serious errors. Element meshes are refined until the acceptable converged solution is obtained. All the columns used for the parametric study are with hinged boundary conditions. All three translations together with the rotation along the longitudinal axis of the section were constrained, while the rotations about other axes were allowed. The numerical simulation consisted of two stages. The analysis was conducted in two steps. The first step consists of a linear eigen-buckling analysis, in order to find the buckling load and modes. After imposing the imperfection, a nonlinear analysis incorporating both geometric and material nonlinearities was then performed using the modified Riks method to obtain the ultimate load of the column. This was achieved by modelling the structure with an initial out-of-plane deflection. The scaled value of linear buckling mode shape was used to create an initial geometric imperfection for the nonlinear post-buckling analysis. The degree of imperfection assumed to have the stage of the buckling mode shape and amplitude is considered as percentage of the member's thickness. For this, the displacement increment method was used. The section was loaded axially at the movable end by prescribing suitable increments of axial displacements. For each incremental step of end-shortening, the total reaction at the end was obtained. Figure 7 shows the mesh patterns and the first buckling mode with boundary conditions for single and starred angles, respectively (Fig. 6).

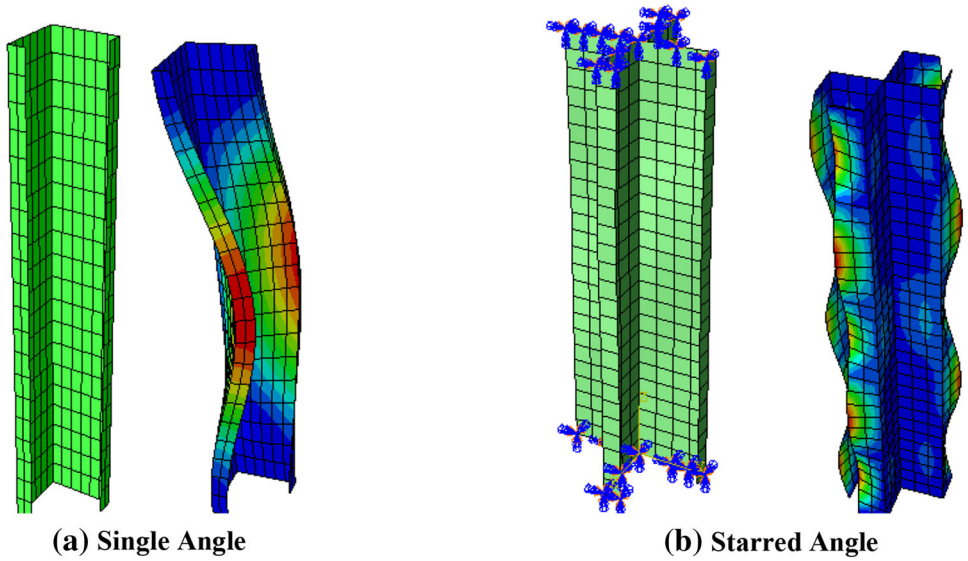

Fig. 6 Meshing and local buckling mode with boundary condition

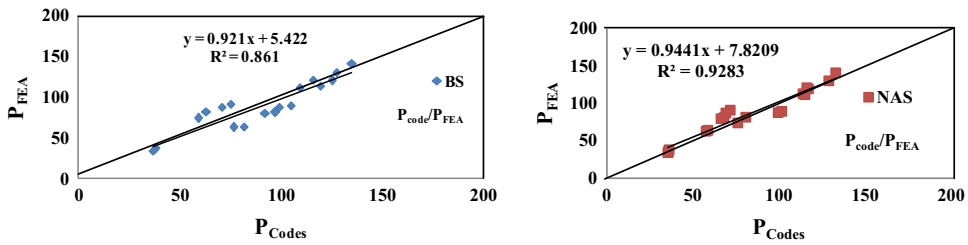

Fig. 7 P_{FEA} versus codal prediction for single angles

One of the factors which affect the ideal behaviour of a column section is the geometric imperfections. These imperfections are induced starting from manufacturing to transportation and also from fabrication. One of the methods of simulating geometrical imperfection is using buckling modes of the specimen. Scaled value of linear buckling mode shape is used to create an initial geometric imperfection for the nonlinear post-buckling analysis. For each incremental step of end-shortening, the total load or reaction at the end is obtained. Pekoz and Schafer [11] suggested that the expression for the average degree of imperfection for the cold-formed steel members is between 0.14t and 0.66t, where t is the thickness of sheet steel. Hence in this study, the results based on the Pekoz's [11] suggested expression were used in finite element analyses. The local buckling imperfection amplitude of 0.25t and the overall imperfection amplitude of L/1000 were used for the axially loaded channels, respectively.

4 Results and Discussion

4.1 Single Angles

Table 2 shows the comparison of experimental and numerical ultimate loads with the unfactored design strength predicted by the various international codes for the single angles under axial compression. In case of single angles with ball-end condition, the predicted ultimate loads by BS: 5950-1987 [1] is higher than the FEA up to 7 %. For single angles with bolted-end condition, the predicted values are higher than the experimental up to 30 %. The mean value of P_{Exp}/P_{BS} for single angles is 0.89, and standard deviation is 0.13. For the single angles, the NAS predicted the ultimate load higher than experimental by 24 %. For a slenderness ratio of 15, the predicted loads agreed well with the experimental results. For angles with bolted-end condition, NAS overestimated the FEA values by 22 %. The mean value of P_{Exp}/P_{NAS} for single angles is 0.95, and standard deviation is 0.12. The comparison between the FEA and the various international codes for the single angles is presented in Fig. 7. As per the study conducted by Young and Ellobody [5], the design rules given by the North American Standards are generally unconservative for short and intermediate column lengths, and for the unequal angles, they prove to be a pioneer for this study done on equal single and starred angles. An equation is proposed for the single angles for both the British Standards and NAS and is as follows:

For single angles $---$ $\mathbf{P_{FEA} = 0.921P_{BS} + 5.42}$ with R^2 of 0.86 [1]

and $\mathbf{P_{FEA} = 0.944P_{NAS} + 7.82}$ with R^2 of 0.93 [2]

Table 2 Comparison of experimental, numerical and theoretical strengths for single angles

Section size	Single angles					
	λ	P_{Exp}	P_{FEA}	P_{FEA}/P_{Exp}	P_{Exp}/P_{BS}	P_{Exp}/P_{NAS}
Ball-end condition						
35 × 35 × 15 × 2	15	36.49	37.99	1.04	0.95	1.01
	20	34.26	35.45	1.04	0.92	0.96
	25	33.82	34.1	1.01	0.92	0.95
40 × 40 × 15 × 2	15	59.2	81.63	1.38	0.94	0.73
	30	53.6	73.87	1.38	0.90	0.70
40 × 40 × 15 × 3.15	15	86.77	91.09	1.05	1.15	1.21
	30	76.1	87.19	1.15	1.07	1.10
Bolted-End Condition						
60 × 60 × 15 × 2	20	59.63	64.09	1.08	0.73	1.01
	30	53.39	62.91	1.18	0.70	0.93
60 × 60 × 25 × 2	20	70.62	81	1.15	0.72	1.04
	30	64.52	79.62	1.23	0.70	0.97
60 × 60 × 15 × 3.15	20	82.63	89.43	1.08	0.79	0.81
	30	76.09	87.66	1.15	0.76	0.76
60 × 60 × 25 × 3.15	20	113.45	119.5	1.05	0.90	0.97
	30	105.02	112.9	1.08	0.87	0.92
70 × 70 × 15 × 3.15	20	120.09	120.9	1.01	1.03	1.03
	30	111.24	111.7	1.01	1.02	0.97
70 × 70 × 25 × 3.15	20	132.56	141	1.07	0.98	1.00
	30	120.15	130.3	1.08	0.94	0.93
Mean				1.12	0.89	0.95
Standard deviation				0.11	0.13	0.12

4.2 Starred Angles

Table 3 shows the comparison of numerical results with the predicted strengths by FEA and various international codes for the starred angles under axial compression. It was observed that for starred angles tested with ball-end condition, the increase in ultimate load is twice when compared to single angles. For short starred angle columns tested with bolted-end condition, the increase in load-carrying capacity is found to be 2.3 times irrespective of the slenderness ratio when compared to single angles. For starred angles with a slenderness ratio of 10, 15 and 25, the prediction of ultimate loads by BS is 4–10 % lower as compared to FEA. For angles with a slenderness ratio of 20 and 30, the prediction was 2–12 % higher than FEA. The NAS underestimated the experimental values tested with ball-end condition by 45 %. The mean values of P_{Exp}/P_{BS} and P_{Exp}/P_{NAS} for starred angles are 0.95 and 1.05, and the standard deviation was 0.06 and 0.13. The comparison between the FEA and the codes for the starred angles is presented in Fig. 8. This study is exclusively done on starred angles which has not been carried out by any other researcher as per the literature study conducted for the past two decades.

An equation is proposed for the starred angles for both the British Standards and NAS and is as follows:

For starred angles $- - - \underline{\mathbf{P_{FEA} = 0.966P_{BS} + 13.03}}$ with R^2 of 0.93 [3]

and $\underline{\mathbf{P_{FEA} = 1.043P_{NAS} + 14.84}}$ with R^2 of 0.95 [4]

5 Load Versus Axial Shortening Behaviour

The load versus axial shortening behaviour is linear initially in most cases up to 50 % of ultimate load irrespective of the cross section of the specimens. As the end-shortening increases and exceeds the critical buckling load, the columns enter the post-buckling range where nonlinear behaviour dominates. In the post-buckling range, the load increases progressively at a slower rate and the end-shortening increases rapidly. This can be noticed as the gradient of the curves is slightly gentler than that at the initial stage. The load ver-

Table 3 Comparison of experimental, numerical and theoretical strengths for starred angles

Section size	Starred angles					
	λ	P_{Exp}	P_{FEA}	P_{FEA}/P_{Exp}	P_{Exp}/P_{BS}	P_{Exp}/P_{NAS}
Ball-end condition						
35 × 35 × 15 × 2	15	78.98	80.19	1.02	0.93	1.10
	20	71.28	79.2	1.11	0.88	1.00
	25	65.19	78.95	1.21	0.88	0.93
40 × 40 × 15 × 2	15	128.55	166.17	1.29	0.99	0.80
	30	123.97	152.07	1.23	1.01	0.84
40 × 40 × 15 × 3.15	15	165.5	165.86	1.00	0.98	1.16
	30	158.9	158.86	1.00	0.97	1.17
Bolted-end condition						
60 × 60 × 15 × 2	20	152.48	169.94	1.11	0.92	1.30
	30	116.9	143.45	1.23	0.97	1.01
60 × 60 × 25 × 2	20	159.46	166.37	1.04	0.96	1.18
	30	156.96	157.16	1.00	1.08	1.20
60 × 60 × 15 × 3.15	20	236.48	238.91	1.01	1.00	1.16
	30	221.98	223.82	1.01	0.98	1.11
60 × 60 × 25 × 3.15	20	264.29	276.52	1.05	0.96	1.13
	30	252.64	271.91	1.08	1.01	1.11
70 × 70 × 15 × 3.15	20	226.01	233.6	1.03	0.85	0.97
	30	215.82	237.93	1.10	0.86	0.94
70 × 70 × 25 × 3.15	20	237.19	298.88	1.26	0.93	0.90
	30	229.55	265.86	1.16	0.92	0.90
Mean				1.10	0.95	1.05
Standard deviation				0.10	0.06	0.13

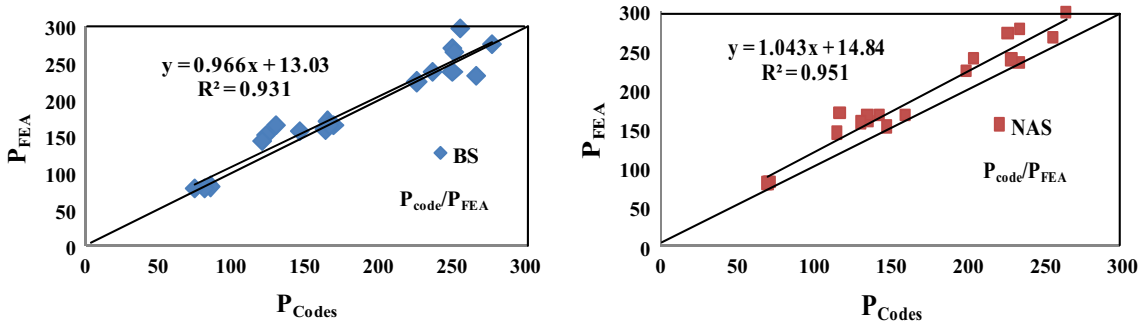

Fig. 8 P_{FEA} versus codal prediction for starred angles

sus axial shortening behaviour of single and starred angles with ball-end condition shows a steeper behaviour for stub columns. The drop in the load is gradual for most of the single angles tested as short columns. Figures 9 and 10 show the load versus axial shortening behaviour of single and starred angles with ball- and bolted-end conditions. It was observed that the behaviour is similar irrespective of the cross section and slenderness ratio for angles with bolted-end condition. The long horizontal plateau after the ultimate load is noticed, indicating high degree of ductility.

6 Modes of Failure

The angles failed by either local plate buckling, flexural buckling about the weak axis, torsional–flexural buckling or torsional buckling. In case of single lipped angles tested as stub columns with bolted-end condition, most of the sections failed by local plate buckling initiated either at the mid-height or at one-fourth height or at the ends both in the FEA and in experimental studies. Single angles tested as short columns with ball-end condition failed by overall flexural buckling.

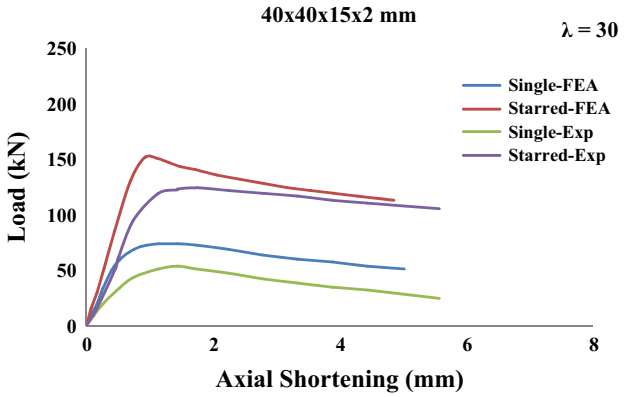

Fig. 9 Axial shortening behaviour of 40 × 40 × 15 × 2 mm with ball-end condition

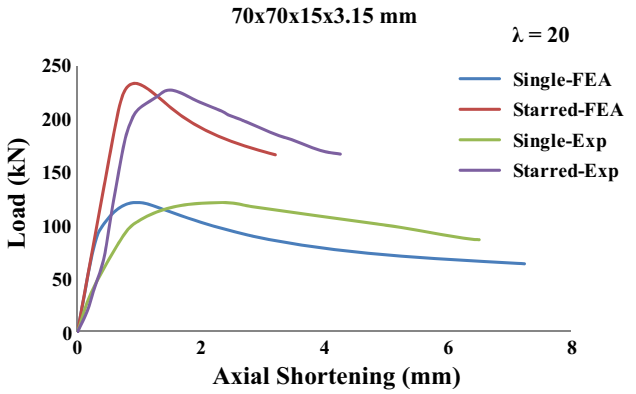

Fig. 10 Axial shortening behaviour of 70 × 70 × 15 × 3.15 mm with bolted-end condition

The failure of these sections occurred always in the flanges of the sections either at mid-height or at one-third height. Single angles tested as short columns with bolted-end condition failed either by flexural or by torsional–flexural buckling. In case of starred angles, the failure is predominantly by torsional buckling irrespective of the slenderness ratio. The failure occurred between the mid- and one-third height of the section in the flanges. In the case of starred angles tested as short columns with bolted-end condition, the failure is by flexural buckling or by torsional buckling. In case of starred angles, local plate buckling was noticed in both FEA and experimental when tested as short columns at mid-height of the section with bolted-end condition. Figure 11 shows the deformed shapes from both the experiment and finite element analysis, which proves that the FEA is a better option in predicting the failure patterns for the cold-formed steel columns.

7 Conclusions

This paper has presented experimental, numerical and analytical study on the behaviour of cold-formed steel single and starred angles subjected to axial compression. The angles are tested with ball- and bolted-end conditions. The column strengths obtained from the experiments are compared with the column strengths predicted by BS: 5950 (Part 5)-1987 and NAS-2007 for cold-formed steel structures and also validated by FEA using ABAQUS 6.10. A total of 38 specimens of nine types of single and starred angle sections are studied with pinned-end conditions. Based on the work done, the following conclusions are drawn:

1. For stub columns with bolted ends, the load-carrying capacity of starred angles increased twice when compared to single angles.
2. Single angles tested as stub columns with ball-end condition failed by local buckling which occurred at mid-height either in the lip or in the flange.
3. In the case of starred angles when tested under ball-end condition, the failure was predominantly by torsional buckling irrespective of the slenderness ratio. The failure occurred in the flanges of the section at one-fourth height.
4. Starred angles when tested under ball-end condition failed by torsional buckling irrespective of the slenderness ratio. The failure occurred in the flanges of the section at one-fourth height.
5. In the case of starred angles, the ultimate loads predicted by the NAS were always higher than the predicted loads by BS.
6. The prediction by the NAS is unconservative for single and starred angles with bolted conditions. The prediction by the BS is always conservative irrespective of the cross section of angles and irrespective of the end conditions whether ball-ended or bolted.
7. In the case of ball-end condition, the predicted ultimate loads by FEA are 5 and 9 % higher than the experimental loads for single and starred angles.
8. FEA overestimated the experimental ultimate loads by 15 and 5 % for single and starred angles.
9. In the case of bolted ends, the predicted loads are lower than the experimental ultimate loads by 2 and 18 % for single and starred angles, respectively.
10. For starred angles tested with bolted-end condition, the values estimated numerically are lower than the experimental values by 18 %.
11. In the case of ball-end condition, the predicted ultimate loads by FEA are 2–38 % higher than the experimental loads for single and starred angles.
12. Change in the end condition played a major role on the ductility behaviour of angles rather than the load-carrying capacity of the section.

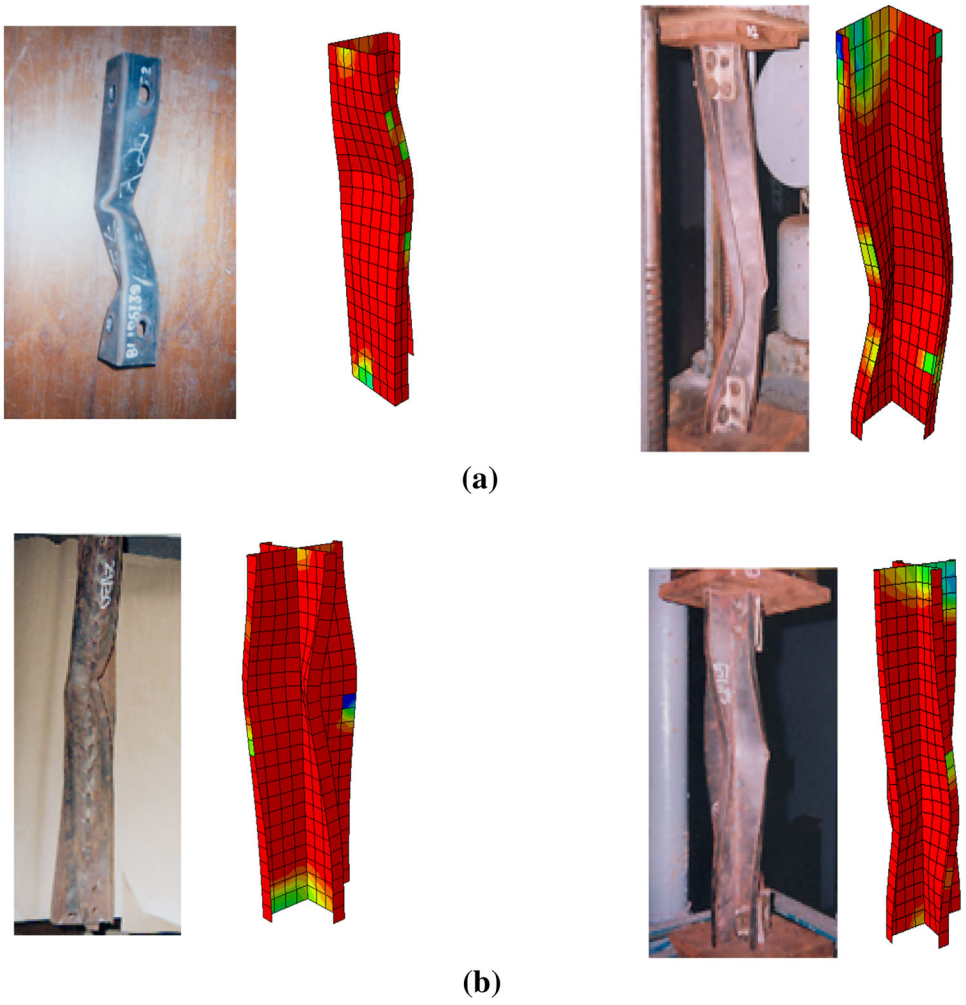

Fig. 11 Experimental and FEA deformed shapes of single and starred angles. **a** Deformed shape for single angle. **b** Deformed shape for starred angle

Annexure: Load-Carrying Capacity in Compression Members

BS: 5950 (Part 5)—1987

Doubly Symmetric Sections

For sections symmetric about both principal axes and closed cross sections which are not subjected to torsional–flexural buckling or braced against twisting, the buckling resistance under axial load P_c is obtained from the following equations.

$$P_c = \frac{P_E\, P_{CS}}{\phi + \sqrt{\phi^2 - P_E\, P_{CS}}} \tag{1}$$

where

$$\phi = \frac{P_{CS}(1+\eta)P_E}{2}$$

where

P_{cs}—short strut capacity = $A_{eff}\ p_y$

A_{eff}—effective cross-sectional area

p_y—the design strength

$$P_E = \frac{\pi^2 EI}{L_E^2}$$

η—Perry coefficient, such that

for $L_E/r \le 20 \quad \eta = 0$

for $L_E/r > 20 \quad \eta = 0.002\,(L_E/r - 20)$

r—radius of gyration corresponding to P_E

Singly Symmetric Sections

For members which have at least one axis of symmetry and which are subjected to torsional–flexural buckling, the ultimate loads are calculated with effective length L_E replaced by a factored effective length αL_E. Where values of α are determined from the following:

$$\begin{array}{lll} \text{For} & P_E \le P_{TF} & \alpha = 1 \\ \text{For} & P_E > P_{TF} & \alpha = \sqrt{(P_{EY}/P_{TF})} \end{array} \tag{2}$$

where

$$P_{\mathrm{E}} = \frac{\pi^2 \mathrm{EI}}{L_{\mathrm{E}}^2} \tag{3}$$

$$P_{\mathrm{TF}} = (1/2\beta)\left[(P_{\mathrm{EX}} + P_{\mathrm{T}}) - \sqrt{(P_{\mathrm{Ex}} + P_{\mathrm{T}})^2 - 4\beta P_{\mathrm{Ex}} P_{\mathrm{T}}}\right] \tag{4}$$

$$P_{\mathrm{E}} = \frac{\pi^2 \mathrm{EI}}{L_{\mathrm{E}}^2} \tag{5}$$

$$P_{\mathrm{T}} = \frac{1}{r_0^2}\left[\mathrm{GJ} + \frac{2\pi^2 \mathrm{EC}_w}{L_{\mathrm{E}}^2}\right] \tag{6}$$

$$\beta = 1 - (x_0/r_0)^2 \tag{7}$$

$$r_0 = \sqrt{\left(r_x^2 + r_y^2 + x_0^2\right)} \tag{8}$$

β and r_0 are calculated using Eqs. (7) and (8), respectively.

NAS Manual: 2007

The nominal axial strength P_n is calculated as follows:

$$P_n = A_e F_n$$
$$\text{Design strength} = P_n/1.80 \text{ ASD}$$
$$= 0.85 \times P_n \text{ LRFD}$$

F_n is determined as follows:

$$\text{For} \quad \lambda_c \le 1.5 \quad F_n = \left[0.658^{\lambda_c^2}\right] F_y \tag{9}$$

$$\text{For} \quad \lambda_c > 1.5 \quad F_n = \left[\frac{0.877}{\lambda_c^2}\right] F_y \tag{10}$$

where

$\lambda_c = \sqrt{\frac{F_y}{F_e}}$ and F_{e} is the least of the elastic flexural, torsional and torsional–flexural buckling stress determined appropriately as follows.

Doubly Symmetric Sections

(i) For doubly symmetric sections, closed cross sections and other sections which are not subjected to torsional or torsional–flexural buckling, the elastic flexural buckling stress, F_e, is determined as follows:

$$F_{\mathrm{e}} = \frac{\pi^2 \mathrm{E}}{(\mathrm{KL}/r)^2} \tag{11}$$

(ii) For doubly symmetric sections subjected to torsional buckling, F_e is taken as the smaller of F_e calculated above and $F_{\mathrm{e}} = \sigma_t$,

where

$$\sigma_{\mathrm{t}} = \frac{1}{\mathrm{Ar}_0^2}\left[\mathrm{GJ} + \frac{\pi^2 \mathrm{EC}_{\mathrm{w}}}{(K_{\mathrm{t}} L_{\mathrm{t}})^2}\right] \tag{12}$$

Singly Symmetric Sections

For singly symmetric sections subjected to torsional–flexural buckling, F_e is taken as the smaller of the following:

$$F_{\mathrm{e}} = \frac{1}{2\beta}\left[(\sigma_{ex} + \sigma_{\mathrm{t}}) - \sqrt{\left[(\sigma_{ex} + \sigma_{\mathrm{t}})^2 - 4\beta\sigma_{ex}\sigma_{\mathrm{t}}\right]}\right] \tag{13}$$

Alternatively, a conservative estimate of F_{e} is obtained using the following equation:

$$F_{\mathrm{e}} = \frac{\sigma_{\mathrm{t}}\sigma_{ex}}{\sigma_{\mathrm{t}} + \sigma_{ex}} \tag{14}$$

where

$$\sigma_{ex} = \frac{\pi^2 \mathrm{E}}{(K_x L_x/r_x)^2} \tag{15}$$

β and r_0 are calculated using Eqs. (7) and (8), respectively, and σ_{t} is calculated using Eq. (15).

References

1. BS: 5950-Part 5.: Structural use of steelwork in building—code of practice for design of cold-formed sections. British Standards Institution (1987)
2. NAS Manual: Cold-Formed Steel Design Manual. American Iron and Steel Institute (2007)
3. Young, B.; Chen, J.: Column tests of cold-formed steel non-symmetric lipped angle sections. J. Constr. Steel Res. **64**, 808–815 (2008)
4. Young, B.: Experimental investigation of cold-formed steel lipped angle concentrically loaded compression members. J. Struct. Eng. **131**(9), 1390–1396 (2005)
5. Young, B.; Ellobody, E.: Design of cold-formed steel unequal angle compression members. J. Constr. Steel Res. **45**, 330–338 (2007)
6. Young, B.; Ellobody, E.: Finite element analysis of cold-formed Steel lipped angle compression members. In: Proceedings of the Fourth International Conference on Advances in Steel Structures. Shanghai, China, pp. 469–478 (2005)
7. Liu, Y.; Chantel, S.: Experimental study of steel single unequal-leg angles under eccentric compression. J. Constr. Steel Res. **67**, 919–928 (2011)
8. Silvestre, N.; Dinis, P.B.; Camotim, M.: Developments on the design of cold-formed steel angles. J. Struct. Eng. **139**(5), 680–694 (2013)
9. Rasmussen, K.: Design of angle columns with locally unstable legs. J. Struct. Eng. **131**(10), 1553–1560 (2005)
10. Shifferawa, Y.N.; Schafer, B.W.: Cold-formed steel lipped and plain angle columns with fixed ends. Thin Walled Struct. **80**, 142–152 (2014)
11. Schafer, B.W.; Pekoz, T.: Computational modelling of cold-formed steel: characterizing geometric imperfections and residual stress. J. Constr. Steel Res. **47**, 193–210 (1998)